Castration Model Illuminates Sex Differences in Healthy Aging: Insights from Metabolome and Transcriptome Analyses

Jianjun Jiang[1,2]*, Na Ge[2], Yuzhi Wang[2], Juntao Qi[3], Guibiao Wen[3], Xiufen Gu[2], Xuewen Yu[4], Muming Shao[4], Yueming Luo[4,5], Kangshuyun Gu[2], Feng Lin[3], Shudong Yang[2]*, and Wei Wei [1]*

[1] Institute for Systems Biology, Seattle, USA;
[2] Department of Nephrology, [3] Department of Urology, [4] Department of Pathology, [5]Department of Geriatrics, Shenzhen Traditional Chinese Medicine Hospital, The Fourth Clinical Medical College of Guangzhou University of Chinese Medicine, Shenzhen, China;

*Corresponding authors:
Jianjun Jiang, Ph.D., E-mail: jjiang@systemsbiology.org
Shudong Yang: ysd0870@gzucm.edu.cn
Wei Wei, Ph.D., E-mail: wwei@systemsbiology.org;

Abstract

Females typically outlive males, a disparity mitigated by castration, yet the molecular underpinnings remain elusive. Our study integrates multi-omics and behavioral analyses to uncover the pivotal compounds and genes influencing healthy aging post-castration, examining serum, kidney, and liver biospecimens from 12-week and 18-month old castrated male mice and their unaltered counterparts. Behavioral tests and LC-MS/MS metabolomics reveal that castrated males exhibit altered steroid hormones, superior cognitive performance, and higher levels of anti-oxidative compounds like taurine, despite identical diets. Integrated metabolome-transcriptome analysis confirms reduced lipid peroxidation and oxidative stress in female and castrated male mice, suggesting a protective mechanism against aging. Histological examinations post-cisplatin treatment highlight the model's applicability in studying sex-dependent drug toxicity and reveal varying susceptibility in organ-specific toxicities, underlining the crucial role of sex hormones in physiological defenses. In essence, our castration model unveils a feminized metabolic and transcriptomic intermediary, serving as a robust tool for studying sex-specific aspects of healthy aging and exploring sex hormone-induced differences in diverse biomedical domains.

INTRODUCTION

Sex-related differences in human are easy to find, where women consistently live longer than men[1]. In the longevous population - centenarians, women always outnumber men[2]. While past research have attributed longer female lifespans to healthier lifestyles, such as lower alcohol and tobacco consumption[2-4], a compiled demographic study of 134 mammal populations across 101 species revealed that females have a median lifespan that is on average 18.6% longer than their male counterparts. This suggests the intrinsic biological mechanisms underlie the sex differences in lifespan[1]. Sex hormones were considered as key factors in explaining the sex difference patterns of longevity[5]. Estrogen was proposed to play protective roles against many diseases, while testosterone may increase the risk of developing diseases and loss of testosterone perhaps promote healthy aging and longevity[6, 7]. Nevertheless, more evidence from clinical trials is needed to elucidate it. Aging stands as a paramount risk factor for a myriad of chronic diseases, with differential impacts on males and females. However, the absence of a stable and broadly applicable model continues to pose a significant challenge in the quest to unravel the intricacies of sex differences in healthy aging[8]. Castration emerges as a potent model for elucidating these sex-based differences in healthy aging. Accumulating evidence suggests that castration can extend the lifespan across multiple mammal species. Notably, historical records indicate that Korean eunuchs had a lifespan extension of 14.4–19.1 years compared to their non-castrated counterparts of similar socio-economic status[9]. Similarly, in veterinary and livestock practices, spaying and castration are recommended for disease prevention and lifespan extension[10]. Despite the widespread applications of castration in these fields, quantitative studies linking castration to healthy aging remained scarce until recent couple of studies. In 2021, Sugrue et al. provided the first evidence of delayed intrinsic aging processes in castrated sheep, as evidenced by a slower DNA methylation clock[11]. Very recently, Jiang et al. showed that castration abolished differences in longevity and growth trajectories between male and female UM-HET3 mice, a genetically diverse strain[12].

Despite these sporadic studies observing the effects of castration on aging, the full extent of castration's role in promoting healthy aging, along with the underlying mechanisms driving sex-specific aging patterns, remain primarily unexplored. This gap is largely attributed to the absence of comprehensive molecular characterization in

castration models. Given that genome sequences retain the same pre- and post-castration, we hypothesize that the alterations in hormone spectrum and subsequent changes in the metabolome, transcriptome, and epigenome induced by castration could be pivotal in regulating healthy aging and extending lifespan. In this study, we present the first integrated multi-omic and behavioral analyses of castrated mice and their non-altered counterparts. We employ mass spectrometry-based targeted and untargeted metabolomics, alongside deep RNA sequencing (RNA-seq), to extensively investigate the multifaceted aspects of sex-related healthy aging associated with castration. Our results implicate several mechanistic insights, laying the groundwork for further detailed investigations and offering a foundation for the development of novel interventions aimed at promoting healthy aging and longevity.

RESULTS

Castration is an effective model of healthy aging

To elucidate the effects of castration on lifespan extension and healthy aging, we employed multi-omics approaches to resolve the potential roles at both molecular and phenotypic levels (**Figure 1A)**. Young adult C57/BL6 mice were castrated at 8 weeks old (casM) and exhibited slower gaining of body weight post-castration, but attained similar body weights as the sham males (shamM) by 60 weeks (**Figure 1B)**. This pattern align with findings in prepubertal castration models using UM-HET3 mice (**Figure 1B)**. At 27-30 weeks of age, we assessed the food intake among the three groups of mice. The casM group exhibited reduced food consumption compared to both shamM and sham female mice (shamF) (**Figure 1C)**. This spontaneous reduction in food intake in casM may contribute to the slower body weight acquisition post-castration, and is particularly intriguing given the well-established benefits of dietary restriction for promoting healthy aging and longevity[13]. Considering the potential impact of testosterone deprivation due to castration on the development of young adult mice, we measured their body length and found no significant difference between casM and sham (**Supplementary Figure 1A**). Similarly, rectal temperature measurements revealed no significant differences among the three groups (**Supplementary Figure 1B**). Notably, hair graying, a common aging marker in both mice and humans[14], was significantly delayed in casM compared to shamM at 13 months, indicating a more youthful phenotype in the castrated group (**Figure 1D**).

Given the known correlation between ages 10 – 14 months in mice and 38 – 47 years in humans, where senescence-related changes become prominent[15], we conducted aging-related behavioral analyses. These included Barnes maze (BM), open field (OF) and novel object recognition (NOR) tasks to evaluate the spatial learning and memory, locomotor activity, and recognition memory in 12 – 13 month-old casM, shamM and shamF mice. Previous studies have shown pronounced cognitive decline in middle-aged mice (8 – 12 months) as assessed by the BM test[16]. However, our results showed that middle-aged casM demonstrated superior performance, spending less time and making fewer errors with less immobile time in locating the escape hole than shamM and/or shamF (**Figure 1E-G**), hinting at a mitigated cognitive decline in casM. Non-significant difference was found in OF and NOR tasks across the three groups (**Supplementary Figure 1C-D**). More than possessing longer lifespans, our results

114 revealed that castration confers a protective effect against cognitive decline. This
115 selective enhancement in spatial learning and memory may reflect the differential
116 influence of castration on brain regions, particularly affecting areas like the
117 hippocampus that are crucial for navigation tasks, while exerting less impact on regions
118 involved in locomotor and recognition memory functions.

119 **Castration affected the secretion of steroid hormone spectrum**

120 Hormones, serving as vital chemical messengers, travel through from bloodstream to
121 tissues for coordinating a range of biological functions, with their dysregulation
122 impacting development[17], aging[18] and disease progression[19]. The effect of surgical
123 castration, specifically the removal of the testes, leads to a marked reduction in
124 testosterone (TS) levels. However, the broader hormone changes resulting from
125 castration remain underexplored. Here, we employed ultra-high-performance liquid
126 chromatography coupled with multiple reaction monitoring tandem mass spectrometry
127 (UHPLC-MRM-MS/MS) to analyze 17 targeted steroid hormones (SHs) in the serum
128 of casM, shamM and shamF mice, four weeks post-operation.

129 Given the limited volume of mouse serum available for SH measurement, we could
130 only detect and compare 10 SH types across three groups. Notably, castration
131 significantly altered SH secretion in casM (**Figure 2A**). As expected, testosterone and
132 its more potent form, dihydrotestosterone, were remarkably reduced in CasM, to the
133 point of being barely detectable (**Figure 2B-C**). Intriguingly, CasM mice exhibited a
134 significant higher level of 17α-Hydroxyprogesterone (17α-OHP) (**Figure 2D**) and
135 lower androstenedione (A4) compared to shamM ($p < 0.05$) (**Figure 2E**). These
136 hormones, precursors to TS, might be part of a compensatory mechanism in response
137 to TS deprivation [20]. In addition, we observed slight increases in aldosterone (ALD)
138 and corticosterone (CORT) in casM, with p-values of 0.11 and 0.083, respectively
139 (**Supplementary Figure 2**). ALD, a mineralocorticoid, and CORT, a glucocorticoid,
140 are primarily produced by the adrenal cortex. Their upregulation may suggest an
141 activated stress response and changes in mineral and glucose homeostasis consequent
142 to TS deprivation.

143 To elucidate metabolites associated with TS, we conducted an untargeted
144 metabolomics analysis by LC-MS/MS on serum samples from three groups of mice,
145 four weeks post-operation. A total of 1495 compounds with MS^2 scores ≥ 0.3 were

identified. Notably, coexpression analysis revealed that 17 of these compounds, which include 11 bioactive lipids, showed a significant correlation with TS levels ($|r| \geq 0.8$, $p \leq 0.001$, **Figure 2F**), These 11 lipids encompass a range of molecules such as prostaglandin B2 (PGD2), a specific phosphatidylcholine (PC) variant, lysophosphatidylserine (LPS), lysophosphatidic acid (LPA), cyclic PA (CPA), glucuronosyldiacylglycerol (GlcADG), sulfurHexosylceramide (SHexCer), and four types of ceramide fatty acids (Cer) (**Supplementary Table 1**). While further investigation is required to solidify these findings, our coexpression analysis suggests that TS deprivation may significantly influence peripheral lipid metabolism, particularly impacting ceramide and lysophosphatide pathways.

Characterization of sex-related serum metabolomic features

To assess the serum metabolomic profile differences among shamM, shamF, and CasM mice at 12 weeks old (12w, 4 weeks post sham/castration procedures), principal component analysis (PCA) was performed using data from 1495 compounds identified by LC-MS/MS (**Figure 3A**). Lipid and lipid-like molecules constituted the largest category (~33%) of these compounds (**Figure 3B**). A comparison of shamM and shamF groups to explore sex-specific differences in serum metabolic activity revealed 255 significantly altered metabolites (SAMs) were identified (**Supplementary Table 2**), with the top SAMs (ranked by fold changes) displayed in **Supplementary Figure 3A.** Despite all mice receiving the same diet, we observed notably higher levels of antioxidants and anti-inflammatory compounds in shamF compared to shamM. These compounds, likely derive from food intake, included carnosic acid[21], arachidonic acid[22], choline[23], nicotinamide[24], D-pantothenic acid[25], gamma-crocetin[26], ruscogenin[27], 4-hydroxycinnamic acid[28], and oleamide[29, 30] (**Figure 3C).** Conversely, shamM mice exhibited elevated levels of metabolites associated with resistance to high-fat diet-related diseases, such as 5-HEPE[31] and 12-HEPE[32], and a higher level of protective L-Anserine[33] than shamF (**Figure 3C)**. Consistently, obesity-related compounds such as LysoPE(0:0/20:3(11Z,14Z,17Z)/0:0) (LysoPE)[34] and 7−Ketocholesterol (7-KC)[35] were found to be lower in male (**Figure 3C)**, offering insights into why obesity is more prevalent in women than men[36].

Differential abundance (DS) score of the 255 SAMs was calculated to inform the overall changes of each pathway (Figure 3D). These SAMs were found to be highly enriched in lipid metabolism related pathways such as “sphingolipid signaling

179 pathway", "regulation of lipolysis in adipocytes" and "arachidonic acid metabolism",
180 suggesting a sex dimorphism in lipid metabolism. Additionally, a serum untargeted
181 metabolomic analysis in the same groups at 18 months old identified 868 compounds,
182 with "lipid and lipid-like molecules" again being the predominant category"
183 (**Supplementary Figure 3B**). PCA analysis suggested that the metabolic profile of 18-
184 month-old casM mice closely resembled that of shamF (**Supplementary Figure 3C**).
185 Similar to the younger mice, older shamF demonstrated higher levels of protective
186 compounds derived from the same diet compared to shamM **(Supplementary Figure**
187 **3D and Supplementary Table 3**), suggesting a potentially stronger ability in females
188 to generate healthy compounds from the same chow.

189 **Metabolomic feminization and taurine enrichment in castrated male mice**

190 In our analysis of 12-week-old mice serum, a comparative study between casM and
191 shamF mice identified 170 SAMs. In contrast, comparisons of "casM *vs* shamM" and
192 "shamF *vs* shamM" revealed 280 and 255 SAMs, respectively (**Figure 4A,**
193 **Supplementary Table 4**). Hierarchical Clustering of the 1495 identified compound
194 demonstrated a closer metabolic profile between casM and shamF than between casM
195 and shamM (**Figure 4B**). These findings, achieved without altering genetic background,
196 suggest that castration feminizes the metabolomic traits of male mice. When ranking
197 these SAMs by fold change (FC), notable differences were observed between shamM
198 and casM. The most significantly upregulated metabolite in casM was the unsaturated
199 fatty acid, PI (16:1/18:2), with $\log_2$FC of 13.14, while the most downregulated was
200 guanosine, with a $\log_2$FC of -6.79. CasM mice exhibited elevated levels of various
201 metabolites associated with healthy aging, anti-skin aging, and anti-inflammation, such
202 as ectoine[37], resolvin D2[38], oleamide[29, 30], taurine[39], taurocholic acid[40],
203 taurodeoxycholic acid[41], nicotinamide[42], ascorbic acid (vitamin C) [43], D-pantothenic
204 acid (vitamin B5)[44, 45] and choline[46] (**Figure 4C**). Similar to shamF, casM mice also
205 showed an enrichment of anti-oxidative metabolites likely derived from plant-based
206 foods, including ganoderenic acid C[47], oleuropeic acid[48], fasciculol C[49], graveoline[50]
207 (**Figure 4C**).

208 Enrichment analysis of the 280 SAMs from the "casM *vs* shamM" comparison
209 categorized them into pathways such as "bile secretion", "vitamin digestion and
210 absorption", "HIF-1 signaling pathway", "pyrimidine metabolism", various fatty acid
211 metabolism pathways including "arachidonic acid metabolism" and "regulation of

212 lipolysis in adipocytes" (**Figure 4D**). Interestingly, lipid metabolism-related pathways
213 were consistently enriched in both the "casM *vs* shamM" and "shamF *vs* shamM"
214 comparisons, indicating a potential sensitivity of lipid metabolism to the levels of SHs.

215 To investigate the metabolomic changes particularly derived from castration,
216 union SAMs among 12w-old casM, shamM and shamF groups were further classified
217 by c-means fuzzy clustering **(Figure 4E**, **Supplementary Table 5**). This analysis
218 revealed that cluster1 metabolites were notably elevated in casM compared to both
219 shamM and shamF. Topology-based pathway enrichment analysis indicated that
220 cluster1 metabolites were significantly ($p < 0.05$) enriched in pathways like "primary
221 bile acid biosynthesis", "D-glutamine and D-glutamate metabolism", "taurine and
222 hypotaurine metabolism" among others (**Figure 4F**). Notably, taurine levels were
223 higher in shamF than in shamM, and castration further augmented taurine levels along
224 with two key components of the taurine and hypotaurine metabolism pathway:
225 taurodeoxycholic acid (TDCA) and taurocholic acid (TCA) (**Figure 4G**). However, in
226 18m-old mice, a higher level of taurine with no significant changes of TDAC and TCA
227 were observed in shamM compared to shamF and casM, (**Figure 4H**), suggesting an
228 age-related sex dimorphism of taurine concentrations in mice serum. Bile acids (BA)
229 are crucial for maintaining lipid homeostasis and have been recognized as significant
230 signaling molecules during aging process[50]. Given that the SAMs from both "casM *vs*
231 shamM" and "shamF *vs* shamM" comparisons were significantly enriched in lipid-
232 related metabolic pathways, and the primary function of taurine is the conjugation of
233 cholesterol into bile acids[51], our findings suggest a potential link between taurine and
234 the sex and/or SH-related differences in lipid metabolism. Taurine, along with TDCA
235 and TCA, serve as antioxidants and protective factors against many degenerative
236 diseases[52]. A recent study has demonstrated that blood taurine levels decline with age,
237 but intake of taurine supplement at middle age can extend the healthy lifespan of mice
238 and monkeys[39]. Considering the established longevity of females and castrated males
239 over unaltered males, our results imply that mice with elevated taurine levels at younger
240 ages may reap more significant benefits than those with higher levels at older ages.

241 **Co-expression analysis across serum, livers and kidneys identifies potential**
242 **taurine-related regulators**

243 Kidney and liver are two major organs of organisms, the sex differences of renal and
244 hepatic function have been aware over years[53]. To elucidate the sex and age-related

245 regulatory networks in kidney and liver functions, we analyzed metabolome and
246 transcriptome of renal cortex and left liver lobe from three groups of mice at 12 week
247 (12w) and 18 months (18m) old. We detected an average of 899 compounds across both
248 tissues, with 121 compounds common among kidneys, livers and serum samples in both
249 age groups of sham, shamF, and casM mice (**Figure 5A** and **Supplementary Table 6**).
250 Coexpression analysis of these 121 commonly detected metabolites (CDMs) revealed
251 4 major clusters (**Figure 5B**). Metabolite Set Enrichment Analysis (MSEA) indicated
252 that Clusters 1, 2 and 3 are primarily involved in "Bile Acid Biosynthesis" and "Glycine
253 and Serine Metabolism" pathways (**Supplementary Figure 4A-C**). Notably, two
254 compounds known for their health-protective properties, taurine and alpha-linolenic
255 acid (ALA), were grouped in Cluster 4. They exhibited a strong correlation ($r > 0.75$, p
256 < 0.01) with adenosine, xanthosine, 1-palmitoylglycerophosphoinositol, L-tyrosine,
257 erythrulose, glycolic acid, PC-M5', pyruvic acid and 5 other lipids include LPC(15:0),
258 LPE(18:2), LPE(20:3), LPS(20:4), FAHFA(18:1/22:3) (**Figure 5C**), suggesting a
259 potential link between Cluster 4 compounds and healthy aging. A recent study has
260 demonstrated that taurine intake can attenuate lipid peroxidative stress (LPOS) and lipid
261 metabolism disorder in mice, evidenced by decreased levels of malondialdehyde
262 (MDA), a marker of LPOS[54]. Similarly, ALA, an omega-3 polyunsaturated fatty acid
263 derived from plants, has also been shown to markedly reduce oxidative stress and
264 increase the lifespan of *Caenorhabditis elegans* in a dose-dependent manner[55].
265 Considering the fact that a linoleic acid-rich diet increases hepatic taurine[56] and the
266 observed strong association (r = 0.934) between taurine and ALA across three sample
267 types from three mouse groups and at two age stages, these results collectively suggest
268 potential role for ALA in taurine-mediated antioxidant defense and lipid metabolism
269 processes.

270 Due to the limited range of lipids identifiable by KEGG compounds database,
271 Cluster 4 compounds were showing enrichment in a few terms include "glyoxylate and
272 dicarboxylate metabolism", "tyrosine metabolism" and others (**Figure 5D**).
273 Noteworthy, xanthosine and adenosine, two key components of "purine metabolism"
274 pathway, were strikingly co-expressed with taurine ($r = 0.973$ and 0.874, respectively,
275 **Figure 5C**). Dysregulated purine metabolism has been implicated in many aging-
276 related disorders such as Alzheimer's diseases[57] and age-associated lower urinary tract
277 dysfunctions[58]. Considering taurine's role in aging delay, we hypothesized that its

influence on lifespan extension might also be linked to xanthosine and adenosine-mediated purine metabolism, though further evidence is required to substantiate this.

Considering the significance of taurine in aging and healthy aging, co-expression analysis and c-means clustering were applied to identify genes that positively associated with taurine. A total of 51 genes, whose expression levels showed similar dynamic trend with taurine across casM, shamM and shamF mice in kidney and liver tissues at both 12w and 18m ages, were identified (**Figure 5E-G**). Among these, 15 genes exhibited a generally decrease in expression in 18m tissues than 12w, such as *Hdac5, Preb, Plk2, Atxn2* and *Trit* (**Figure 5E**). Two key lipid metabolism genes, *Srebf1* and *Ppard* were among the 51 taurine-associated genes. *Srebf1* encodes sterol regulatory element-binding protein 1 (SREBP1), a critical transcription factor regulating lipogenes involved in fatty acid and cholesterol biosynthesis[59]. *Ppard* encodes Peroxisome proliferator-activated receptor-delta (PPAR-δ), a member of the PPAR group in the nuclear receptor superfamily, known for its ligand-binding domains (LBD) that interacts with a broad range of lipid and lipid-like molecules[60]. This includes multiple types of polyunsaturated fatty acids, such as arachidonic and linoleic acid[60]. Both PPAR-δ and SREBP1 are also involved in retinoid X receptors/ Vitamin D Receptor (RXR/VDR) pathway (**Supplementary Table 7**). Given previous research showing that intestinal-specific deletion of VDR increased taurine levels[61], it is posited that taurine may also be associated with PPAR-δ and SREBP1 involved RXR/VDR pathway. Taken together, our results from both metabolomics and RNA-seq analysis strongly suggest that taurine is a key regulator in lipid peroxidation and metabolism, potentially playing a significant role in the process of healthy aging.

Joint metabolomic-transcriptomic analysis reveals a stronger capacity of defensing lipid peroxidation in female and castrated male

From deep RNA-seq analysis, we identified differentially expressed genes (DEGs) among casM, shamM and shamF groups in kidney and liver tissues (**Figure 6A-B, Supplementary Table 6**). In the kidneys of 12w old mice, over 4500 DEGs were noted in the comparisons of "shamF *vs* shamM" and "casM *vs* shamM," while only 987 genes showed differential expression between shamF and casM. Interestingly, livers seemed to be less affected by sex and/or the changes of SH levels than kidneys as only 2053 and 2533 DEGs were detected in “shamF *vs* shamM” and “casM *vs* shamM” comparisons, respectively, in 12w-old mice, and 546 DEGs between shamF and casM.

311 Hierarchical clustering of RNA-seq data also revealed that the transcriptomic profiles
312 of casM samples more closely resembled those of shamF than shamM samples, with
313 the exception of 18m-old livers, suggesting a feminizing effect of castration that creates
314 a crossover zone between male and female transcriptomic profiles in both kidney and
315 liver (**Figure 6C**). However, the impact of sex and/or SH levels on transcriptomes,
316 pronounced at 4 weeks post-castration, appeared to diminish in 18-month-old mice. In
317 this older age group, the numbers of DEGs among the 3 groups were reduced, especially
318 the comparisons of shamM with casM. In 18-month-old kidneys and livers of "casM *vs*
319 shamM", it showed only 435 and 353 DEGs, respectively.

320 Mapping the DEGs onto mouse chromosomes, we found that DEGs in "shamF *vs*
321 shamM" and "casM *vs* shamM" from both 12w and 18m-old liver tissues were
322 significantly clustered to chr4B3 (FDR < 0.05). Of the 145 annotated genes in chr4B3,
323 46 belong to the Major Urinary Proteins (*Mup*) family, with 25 being pseudogenes.
324 Except for *Mup4* and *Mup5*, which were barely detectable, the other *Mup* family genes
325 in chr4B3 were drastically reduced in casM and shamF livers, showing an average
326 log2FC = -5.57 (**Supplementary Figure 5A**). *Mup14*, *7*, *11*, and *1* were the top 4
327 differentially expressed *Mup* genes. It is known that *Mup* genes, predominantly
328 expressed in the liver, exhibit sexually dimorphic traits. Male mice typically excrete 2–
329 8 times more Mup protein in their urine compared to females [62]. Our results indicate
330 that the expression of *Mup* genes is influenced not only by sex genotypes but also by
331 testosterone levels.

332 To identify potential long-term salutary regulatory elements brought by sex and/or
333 castration at old age, we conducted a joint metabolomic-transcriptomic analysis. Here,
334 shamM mice, typically having a shorter liferspan, served as controls, while shamF and
335 casM mice, associated with healthier and longer lifespans, were the focus [63]. We utilized
336 the SAMs and DEGs from "shamF *vs* shamM" for the joint analysis to investigate
337 female-specific signatures; meanwhile, the joint metabolomic-transcriptomic analysis
338 was also performed using the SAMs and DEGs from "casM *vs* shamM" for interpreting
339 castration-specific features. In 18m-old kidneys, both shamF and casM groups showed
340 enrichment in KEGG programs related to "lysosome" and "cholesterol metabolism"
341 (**Supplementary Table 8-9**). In the liver of the same age group, the significantly
342 enriched KEGG pathways in the "casM *vs* shamM" comparison are illustrated in
343 **Figure 6D**. Notably, 20 terms, such as "linoleic acid metabolism", "arachidonic acid

344 metabolism", "retinol metabolism", "Jak-stat3 signaling" and "glutathione metabolism"
345 were consistent with those in the "shamF *vs* shamM" comparison (terms marked by
346 orange in **Figure 6D and 6E, Supplementary Table 10-11**). These KEGG terms are
347 known to play critical roles in lipid peroxidation.

348 To further validate these findings, we measured levels of malondialdehyde (MDA)
349 - a final product of polyunsaturated fatty acids peroxidation, in the three groups of mice.
350 Results indicated that shamF mice exhibited the lowest, while shamM mice had the
351 highest MDA levels in 18m-old livers, suggesting that females and castrated males
352 experience less lipid oxidation stress than their male counterparts (**Figure 6F**).
353 Additional oxidative stress markers, SOD1 and SOD2, were also tested and showed
354 similar trends to MDA among three groups (**Supplementary Figure 5B**). Taken
355 together, our analysis suggests a close association between lipid metabolism and sex
356 and SH levels. CasM and shamF mice are likely to absorb more health-beneficial
357 compounds from their diet and experience reduced lipid peroxidative stress, potentially
358 contributing to their longer lifespans.

359 **Evaluating sex-dependent cisplatin toxicity through castration models**

360 The clinical application of anti-tumor drugs, particularly Platinum-based drugs (PBDs)
361 like cisplatin, which are used in nearly half of all chemotherapy treatments[64], is often
362 hindered by drug-induced tissue toxicity. Notable adverse effects of these drugs include
363 nephrotoxicity and hepatotoxicity, exhibiting differential impacts between male and
364 female patients[65]. Such sex-dependent disparities in toxicity may be influenced by SHs,
365 as suggested by the increased risk of nephrotoxicity observed in perimenopausal
366 women undergoing cisplatin treatment[66]. Aging, a key factor influencing SH levels in
367 both sexes, further complicates this relationship. To evaluate the utility of the castration
368 model in studying the role of SHs in sex-dependent toxicity, we treated 12w-old mice
369 (4 weeks post-castration/sham procedure) with a low dose of cisplatin twice, every 72
370 hours. Given that the kidney, and to a lesser extent the liver, are particularly vulnerable
371 to cisplatin-induced damage, we conducted histological analyses on the renal cortex
372 and left liver lobe tissues post-treatment.

373 Hematoxylin and eosin (H&E) staining of liver tissues showed the most severe
374 liver injury in shamF mice, characterized by marked steatosis, sinusoidal congestion,
375 and hemorrhage. In contrast, sham-operated male (shamM) and castrated male (casM)

mice displayed comparatively less hepatic damage (**Figure 6G**). Conversely, Periodic Acid Schiff (PAS) staining of kidney tissues showed that casM mice had more severe kidney damages than both shamF and shamM, with a notable increase in acute renal tubule injury (**Figure 6H**). Previous studies on cisplatin-induced hepatotoxicity have yielded limited insights regarding sex differences. However, substantial evidence indicates that males are more susceptible to cisplatin-induced nephrotoxicity[65]. Studies administering cisplatin to rats at both 2 weeks (1 mg/kg/day) and a single dose (7.5 mg/kg) have shown that males experience more severe nephrotoxic effects than females[67]. Our pathological observations, combined with previous findings and the fact that castrated male (casM) mice have the lowest testosterone (TS) levels, suggest that intermediate TS levels, similar to those in shamF mice, may offer greater protection against renal toxicity induced by cisplatin.

DISCUSSION

The burgeoning aging population has become a global concern, poised to increase the prevalence of age-related diseases[68]. Hence, it is imperative to gain a better understanding of the regulatory factors contributing to healthy longevity. Historically, sexual dimorphism in aging has been largely overlooked, despite the fact that females consistently outlive males. While the practice of castration, known to prolong the lifespan in domesticated dogs and cats in veterinary medicine[69], offers intriguing possibilities for aging research, its potential has only recently begun to be explored. However, existing studies on this subject are isolated and primarily focus on the decelerated methylation clock and lifespan extension following castration, offering scant insights into the underlying molecular regulations[11, 12, 70, 71]. Consequently, the utilities of castration as a model to dissect sex differences in healthy aging and to elucidate the underlying molecular mechanisms remain largely unexplored.

In this study, we integrated observational investigations, behavioral tests and multi-omics approaches to systematically investigate sex differences in lifespan across different stages of mice. We found that adult casM mice spontaneously consumed less food than shamM, a behavior we believe to be the primary factor contributing to their reduced rate of body weight gain. Considering the well-established connection between dietary restriction, body weight, overall health, and longevity[13, 72], it is plausible to suggest that this dietary pattern confers benefits for healthy aging in casM mice. The underlying triggers prompting reduced food intake in casM mice merit further

409 investigation. Intriguingly, despite identical diet, shamF and casM mice exhibited
410 elevated levels of multiple food-derived health-promoting compounds compared to
411 shamM, including taurine, recently known for its aging-slowing effects in various
412 species[39]. These findings point to a potential influence of the gut microbiome in
413 modulating host metabolism and appetite regulation[73], which in turn can affect eating
414 behaviors and the bioavailability of beneficial compounds in food. Given the dynamic
415 interplay between the gut microbiome, aging, and its sex-dependent modulation[74, 75],
416 our results hint at the involvement of sex hormones in shaping the microbial community.
417 This, in turn, could influence dietary behaviors and the assimilation of protective
418 compounds from food. Future research delving into the microbiota-gut-brain axis and
419 its relationship with healthy aging in this castration model is warranted.

420 Previous research has offered mixed insights into the impact of castration on
421 cognitive function. One such study employed a dual-task approach – utilizing an 8-arm
422 radial maze and a step-down avoidance task – to assess spatial and short-term memory
423 in rats. Conducted approximate 82 days post-surgical and chemical castration, the study
424 concluded that castration deteriorates memory function[76]. In contrast, our findings,
425 based on BM test in castrated mice, suggest an enhancement in cognitive performance.
426 Several factors could account for these divergent outcomes. First, the timing of
427 cognitive assessments post-castration differed between the studies. Our behavioral tests
428 were performed on 12-13month old mice, nearly 10-11 months after castration or sham
429 operations. It is plausible that the benefits of castration on spatial memory may not be
430 readily apparent in younger rodents but become more pronounced with age. Second,
431 the choice of behavioral tasks could also contribute to the observed discrepancies. The
432 step-down inhibitory avoidance task, employed in the previous study, uses immediate
433 electric shocks as stimuli to evaluate aversive memory, while the 8-arm radial maze
434 task requires deprivation of food and/or water for animals. Electric shock is a type of
435 psychological stress for rodents[77]. Mounting evidence suggests that testosterone
436 significantly modulates physiological responses to stressors[78]; thus, the markedly
437 reduced testosterone levels in castrated mice could potentially confound the evaluation
438 of cognitive performance. To mitigate potential confounders, we opted for less stressful
439 tasks – namely BM, OF and NOR tests. Our results from the BM test indicate that
440 castration not only extends lifespan but also attenuates cognitive decline in older mice.
441 This suggests that the castration model offers a nuanced understanding of aging, one

that incorporates both longevity and cognitive preservation.

Sex as a key determinant biological variable has been historically overlooked despite sexual dimorphism can be observed everywhere. On one hand, the bias toward using male subjects in biomedical research has often been justified by the desire to minimize variability, particularly traits influenced by the female estrous cycle[8]. This male-centric focus has inadvertently limited our understanding of tissue function and disease mechanisms from a sex-specific perspective, thereby highlighting the pressing need for more inclusive animal models. On the other hand, straightforwardly comparing male with female is generally applied in the increasingly emphatic but still limited sex-difference studies, which made the leading mechanisms hard to recognize due to complicated variables between male and female in both genetic and non-genetic aspects. To broaden the feasibility and practicability of applying the castration model in sex-dependent biological queries, we investigated the differences in tissue injuries induced by tumor drugs among three groups of mice. While more severe renal damages have previously been observed in males compared to females following cisplatin treatment at both young and old ages[79], the specific roles of genetic and non-genetic co-determinants in this disparity are still elusive. Rostami et al. reported that rats, 1 week post-castration and treated with a low dosage of TS rather than high dosage, exhibited increased tolerance to cisplatin nephrotoxicity[80]. Complementing this, our pathological assays showed that castration alone, without TS treatment, exacerbated renal toxicity. These findings collectively suggest that balanced levels of TS are essential in defending against such toxicity. Given that aging is a major contributor to changes in SH levels in both sexes[6, 81], and considering the significant impact of these changes on chemotherapy-induced toxicities, there is an imperative need for more comprehensive research to integrate these hormonal alterations with chemotherapy toxicity across various age groups, thereby enhancing the understanding and management of chemotherapy side effects in the aging population.

In summary, our study, along with several past work[11, 12], collectively underscore the versatility of the castration model and its untapped potential in elucidating sex differences in healthy aging. The model effectively "feminizes" males at multiple molecular levels through alterations in SHs, while preserving the somatic male genotype. This unique duality positions the castration model as a useful tool for distinguishing between hormone-induced sex differences and genotypic sex,

475 broadening its utility beyond the scope of aging research.

476

METHODS

Animals, surgical castration procedures, and sample collections

C57/BL6 mice were purchased from Zhuhai BesTest Bio-Tech Co,.Ltd. and housed in the animal facility of Shenzhen TopBiotech Co., Ltd (Shenzhen, China) under pathogen-free condition with free access to chow and water. Male and female mice at 8 weeks old were anesthetized by isoflurane for castration (testicles removed) or sham procedures. Mice were placed on a warm pad after suture, then transferred to cages while awake. 4-weeks post-castration/sham operations, serum was collected for steroid hormone detection and untargeted metabolites analysis while liver and kidney were dissected for untargeted metabolites analysis and RNA-seq (n=3-6/group). Castrated/sham mice at 12-13m old were subjected to behavioral tests and were sacrificed for sample collection at 18m. At 18m, serum was used for untargeted metabolomics while liver and kidneys were dissected for both untargeted metabolomics and RNA-seq (n=3-6/group). The animal study protocol was approved by the Animal Ethics Review Board of Shenzhen TopBiotech Animal Facilities (No. TOP-IACUC-2021-0100).

Food intake, body length and rectal temperature measurement

To investigate the potential link between reduced food intake and slower body weight gain in castrated male mice (casM), we monitored the weekly changes in chow weight over a 4-week period in 3 cages per group, each housing 3-5 mice aged 27 weeks. The average food intake per mouse was calculated on a weekly basis. In assessing the impact of castration on growth, we measured the body lengths of 29-week-old casM (n = 13), shamM (n = 12), and shamF (n = 13) mice. Mice were gently extended to full length, and measurements were taken from apex nasi to the base of the tail (tail not included). Additionally, rectal temperature was measured on 30 weeks and 32 weeks old casM (n = 13), shamM (n =12) and shamF (n = 13) mice, with the data combined for subsequent analysis. Statistical differences in food intake, body length, and rectal temperature across the three groups were evaluated using one-way ANOVA, multiple comparisons with Tukey correction.

Behavioral tests

Three groups of mice include casM, shamM and shamF at 12-13 months old (n= 6-13) were subjected to BM, OF and NOR tasks. A 60 cm high, 120 cm-diameter and 60 mm

509 thick circular wheeled PVC slab with 25 cm-diameter holes was used for BM tests. A
510 modified protocol was employed following the standard methods in previous study[82].
511 Briefly, mice were firstly trained in continuous 7 days to find the escape hole within 4
512 mins; if failed, mice were finally guided to the target hole gently. Mice were subjected
513 to the probe trial on day 8. OF test was applied to test the exploratory behavior and
514 general activity of mice, mice were placed in an enclosure, rectangular tank with
515 surrounding walls for 5 mins, distance moved, time spent moving, rearing, and change
516 in activity over time for each mouse were recorded. NOR test was performed following
517 previous study[83]. Mice were placed in the empty tank for 10 mins on day1; day 2, two
518 objects were placed in the tank, and mice were allowed for 10 mins to explore; one of
519 the objects was replaced by a new one on day 3, and time spent for exploration (TE)
520 within 5 mins for each object was recorded. NOR index was calculated via this
521 formulation: NOR index = new object TE- old object TE/ Total TE. Mice behaviors
522 during these tests were recorded and analyzed by ANY-MAZE software
523 (https://www.any-maze.com/). Statistical differences in BM, OF and NOR tasks among
524 the three groups were analyzed via one-way ANOVA, multiple comparisons with
525 Turkey correction.

526 **Sample treatment for targeted steroid hormone spectrum detection**

527 50 μL serum was thawed and vortexed for 30s following by mixture with purified H_2O,
528 internal standard working solution and methanol. The well mixed samples were then
529 subjected to repeated 13000 rpm centrifuge for 10 minutes (mins) under 4°C. The
530 supernatant was retained further purified with OASIS PRiME HLB uElution (SPE).
531 200 μL methanol and 200 μL H_2O were separately used to wash and equilibrate the SPE
532 cartridges. The supernatant was loaded to the equilibrated cartridges and then washed
533 by 200 μL 10% ACN/H_2O (v/v) and 200 μL Hexane. The flow-through fraction was
534 discarded. Rinse the cartridge was with 40 μL 90% ACN/H_2O (v/v) and collect the
535 cluent. Add 60 μL H_2O to the cluent and shake the mixture for 3 mins. The final mixture
536 and the same volume of isotopically-labelled internal standards were subjected to
537 UHPLC-MS/MS analysis.

538 **Serum sample preparation for untargeted MS analysis**

539 150 μL methanol which was premixed with isotopically-labelled internal standard
540 compounds was added to 50 μL mouse serum and vortexed for 30 seconds to mix well.

541 The mixture was then sonicated for 10 mins in ice water bath and incubated for 1 h at -
542 40 °C to precipitate proteins. After 15-min high-speed centrifugation, the supernatant
543 was used for MS analysis. An equal aliquot of the supernatants obtained from each
544 serum sample was mixed as the quality control (QC).

545 **Kidney/liver sample preparation for untargeted MS analysis**

546 10-25 mg tissues were submerged with extraction solution (methanol:water = 3: 1, with
547 isotopically-labelled internal standard mixture) and homogenized in ice-water bath.
548 Incubate homogenized samples for 1 h at -40°C and centrifuge at 12000 rpm for 15 min
549 at 4°C. The supernatant was retained for MS analysis. A volume matched quality control
550 (QC) sample was prepared for MS.

551 **UHPLC-MS/MS analysis for targeted steroid hormone spectrum**

552 EXIONLC System (Sciex) equipped with a Waters Acquity Uplc Bch C8 column was
553 utilized for UHPLC analysis at Biotree Technology Co., Ltd, Shanghai, China. Assay
554 development was applied by SCIEX 6500+ triple quadrupole mass spectrometer (Sciex)
555 with an IonDrive Turbo V electrospray ionization (ESI) interface, under multiple
556 reaction monitoring (MRM) module. MassLynx Work Station Software (Version 4.1)
557 was employed for MRM data acquisition and preprocessing.

558 **UHPLC-MS/MS untargeted metabolomics analysis**

559 T3 chromatographic column with affinities to both lipid and hydrophile at Biotree
560 Technology Co., Ltd (Shanghai, China) was used to acquire the metabolome of
561 castrated male (casM), sham male (shamM) and sham female (shamF) mice by Orbitrap
562 mass spectrometer. Joint negative (NEG) and positive (POS) ionization modes were
563 employed for detecting metabolites based on their mass to charge ratios. Raw data was
564 converted to the mzXML format using ProteoWizard platform
565 (https://proteowizard.sourceforge.io/) and processed with an in-house R script and
566 XCMS tool[84] for peak detection, extraction, alignment, and integration. Data was
567 subjected to fragment extracted ion chromatogram (MS^2) annotations as previously
568 described[85], MS^2 metabolites with scores > 0.3 were retained for next-step analysis.
569 These compounds were mapped to Human Metabolome Database (HMDB) and
570 classified into multiple categories. The biggest category under both NEG and POS
571 modes is lipid and lipid-like molecules, which counts for ≥ 30% identified metabolites
572 (**Figure 3a-b, Supplementary Table 2-3**). Compounds from NEG and POS modes

573 were merged for down-stream analysis.

574 **RNA extraction for RNA-seq analysis**

575 Total RNA was extracted using Trizol reagents (Invitrogen Cat#15596026) as we have
576 described before[86]. PolyA-tailed RNA was enriched for constructing 150bp pair-end
577 RNA-sequencing libraries using MGISEQ-2000RS kit (MGI Cat#1000012555), and
578 sequenced by DNBseq MGI2000 platform at BGI genomics Co., Ltd, Shenzhen, China.

579 **Cisplatin administration**

580 Mice were administrated for intraperitoneal injection of cisplatin (Cat# 232120, sigma)
581 at 4 weeks post-castration/sham operations, with a dosage of 5 mg/kg every 72 hours
582 for 2 times. Mice were sacrificed 48 hours after cisplatin treatment for the collection of
583 liver and kidney tissues.

584 **Histopathological analysis**

585 For liver and kidney tissue examination, samples were first fixed in 10% formalin
586 solution for 48 hours, followed by paraffin embedding. Sections of 3 μm thickness were
587 then prepared for histological analysis. Hematoxylin and Eosin (H & E) and Periodic
588 Acid-Schiff (PAS) staining were performed according to established protocols. Liver
589 injury was evaluated by visually inspecting the patterns of steatosis, sinusoidal
590 congestion, and hemorrhage. Renal injury was quantitatively assessed using the scoring
591 criteria established in a previous study[87]. Statistical differences of renal injury scores
592 across the three groups were assessed one-way ANOVA (multiple comparisons with
593 Turkey correction).

594 **Western-blot**

595 Total protein was isolated on ice by cell & tissue lysis buffer (Cat#P0013, Beyontime,
596 China) and quantitated using BCA assay kit (Cat#P0012, Beyontime, China).
597 Approximate 15ug protein was used for western-blot assays following previous
598 protocols[68]. Antibodies for MDA, SOD1 and SOD2were purchased from abcam (Cat#
599 ab243066, ab13498 and ab13533), GAPDH was purchased from Beyontime (Cat#
600 AF0006).

601 **Identification of significant altered metabolites (SAMs) and differentially**
602 **expressed genes (DEGs)**

603 A strict pipeline was applied to identify SAMs. Firstly, the normalized peak values of

604 metabolites were subjected to unsupervised principal component analysis (PCA) and
605 then administrated to supervised orthogonal projections to latent structures-
606 discriminate analysis (OPLS-DA) for data modeling by commercial SIMCA software
607 (V16.0.2). A 7-fold cross validation was employed for model selection. To evaluate the
608 predictive power and robustness of OPLS-DA model, a 200-times-permutations was
609 performed and the value of variable importance in the projection (VIP) of the first
610 principal component in OPLS-DA analysis was calculated which represents the
611 contribution of each variable to the model. Metabolites with VIP > 1 and students' t-
612 test *p*-value < 0.05 were recognized as SAMs. For DEG identification, quality control
613 was performed for raw RNA-seq reads by SolexaQA (-h 30, -l 30)[88]. Cleaned reads
614 were subjected to Hisat2[89] for mapping. Cufflinks package[90] was utilized to calculate
615 the Fragments Per Kilobase of transcript per Million mapped reads (FPKM) values and
616 to identify DEGs use FDR < 0.05 as the cutoff value.

617 **Expression trend clustering analysis**

618 To identify expression trend patterns of metabolites among the serum samples of 12w
619 casM, shamM and shamF, the union of SAMs across three pairwise comparisons in
620 **Figure 4E** were analyzed by Mfuzz package (c=9, m =1.25)[91]. To illustrate genes that
621 potentially related with taurine, the expression levels (FPKM values) of all the
622 annotated genes in kidneys and livers at 12w and 18m casM, shamM and shamF mice,
623 were also subjected to Mfuzz package[91] for clustering (c=9, m =1.25). The semi-
624 quantitative concentrations of taurine were plotted as stack lines. Genes that show
625 similar expression trend with taurine in all the tissues were retained (**Figure 5F-G**).

626 **Hierarchical clustering analysis**

627 Hierarchical clustering analysis for SH levels after castration/sham treatments (Figure
628 2A), the expression of 51 taurine related genes (**Figure 5E**), serum metabolomic
629 profiles among casM, shamM and shamF using (**Figure 4B**) and tissue RNA-seq gene
630 expression profiles (Figure 6C), were performed by Hclust function in R platform using
631 Euclidean distance metric and complete lineage. The z-score standardized SH levels
632 and expression levels of taurine related genes after clustering were visualized via
633 heatmap using pheatmap 1.0.12 package.

634 **Enrichment analysis of SAMs**

635 SAMs were subjected for topology-based KEGG pathway enrichment analysis using

MetaboAnalyst with default parameters[92]. Differential abundance (DA) scores[93] were calculated for the significant enrichment terms using this formula: DA scores = $\frac{\text{Up regulated metabolite No.in the pathway} - \text{Downregulated metabolite No. in the pathway}}{\text{Total metabolite No.of the pathway}}$

Joint metabolome & transcriptome analysis

To examine the interplay between metabolomics and other transcriptomics layers, SAMs and DEGs were used for joint metabolome & transcriptome enrichment analysis against KEGG pathways via MetaboAnalystR under joint-analysis module by hypergeometric test with default parameters. FDR < 0.05 was applied as the cut-off value.

REFERENCE

1. Lemaître, J.-F. et al. Sex differences in adult lifespan and aging rates of mortality across wild mammals. *Proceedings of the National Academy of Sciences* **117**, 8546-8553 (2020).
2. Martínez-Sellés, M. et al. Sex-Related Differences in Centenarians and Their Hearts. *J Am Geriatr Soc* **64**, 444-446 (2016).
3. Evert, J., Lawler, E., Bogan, H. & Perls, T. Morbidity profiles of centenarians: survivors, delayers, and escapers. *J Gerontol A Biol Sci Med Sci* **58**, 232-237 (2003).
4. Miszko, T.A. et al. Effect of strength and power training on physical function in community-dwelling older adults. *J Gerontol A Biol Sci Med Sci* **58**, 171-175 (2003).
5. Marais, G.A.B. et al. Sex gap in aging and longevity: can sex chromosomes play a role? *Biol Sex Differ* **9**, 33 (2018).
6. Horstman, A.M., Dillon, E.L., Urban, R.J. & Sheffield-Moore, M. The role of androgens and estrogens on healthy aging and longevity. *J Gerontol A Biol Sci Med Sci* **67**, 1140-1152 (2012).
7. Iorga, A. et al. The protective role of estrogen and estrogen receptors in cardiovascular disease and the controversial use of estrogen therapy. *Biol Sex Differ* **8**, 33 (2017).
8. Mauvais-Jarvis, F., Arnold, A.P. & Reue, K. A Guide for the Design of Pre-clinical Studies on Sex Differences in Metabolism. *Cell Metab* **25**, 1216-1230 (2017).
9. Min, K.J., Lee, C.K. & Park, H.N. The lifespan of Korean eunuchs. *Curr Biol* **22**, R792-793 (2012).
10. Howe, L.M. Current perspectives on the optimal age to spay/castrate dogs and cats. *Vet Med (Auckl)* **6**, 171-180 (2015).
11. Sugrue, V.J. et al. Castration delays epigenetic aging and feminizes DNA methylation at androgen-regulated loci. *Elife* **10** (2021).
12. Jiang, N. et al. Prepubertal castration eliminates sex differences in lifespan and growth trajectories in genetically heterogeneous mice. *Aging Cell*, e13891 (2023).
13. Wilson, K.A. et al. Evaluating the beneficial effects of dietary restrictions: A framework for precision nutrigeroscience. *Cell Metabolism* **33**, 2142-2173 (2021).
14. Zhang, Z. et al. Wnt/β-catenin signaling promotes aging-associated hair graying in mice. *Oncotarget* **8**, 69316-69327 (2017).
15. Bresilla, D. et al. The sex-specific metabolic signature of C57BL/6NRj mice during aging. *Sci Rep* **12**, 21050 (2022).
16. Raldiris, T.L., Perez, E., Donovan, E.K. & Dzierzewski, J.M. Cognitive control beliefs and cognitive functioning in mid- to late-life. *Br J Dev Psychol* **39**, 269-281 (2021).
17. Kraemer, W.J., Ratamess, N.A., Hymer, W.C., Nindl, B.C. & Fragala, M.S. Growth Hormone(s), Testosterone, Insulin-Like Growth Factors, and Cortisol: Roles and Integration for Cellular Development and Growth With Exercise. *Front Endocrinol (Lausanne)* **11**, 33 (2020).
18. van den Beld, A.W. et al. The physiology of endocrine systems with ageing. *Lancet Diabetes Endocrinol* **6**, 647-658 (2018).
19. Crafa, A. et al. The Burden of Hormonal Disorders: A Worldwide Overview With a Particular Look in Italy. *Front Endocrinol (Lausanne)* **12**, 694325 (2021).

20. Turcu, A., Smith, J.M., Auchus, R. & Rainey, W.E. Adrenal androgens and androgen precursors-definition, synthesis, regulation and physiologic actions. *Compr Physiol* **4**, 1369-1381 (2014).
21. Lin, C. et al. Effects on longevity extension and mechanism of action of carnosic acid in Caenorhabditis elegans. *Food Funct* **10**, 1398-1410 (2019).
22. Das, U.N. Ageing: Is there a role for arachidonic acid and other bioactive lipids? A review. *J Adv Res* **11**, 67-79 (2018).
23. Wortmann, S.B. & Mayr, J.A. Choline-related-inherited metabolic diseases-A mini review. *J Inherit Metab Dis* **42**, 237-242 (2019).
24. Igarashi, M. et al. Chronic nicotinamide mononucleotide supplementation elevates blood nicotinamide adenine dinucleotide levels and alters muscle function in healthy older men. *npj Aging* **8**, 5 (2022).
25. Hong, Y. et al. Association between plasma Vitamin B5 levels and all-cause mortality: A nested case-control study. *J Clin Hypertens (Greenwich)* **24**, 945-954 (2022).
26. Mohammadi, E., Mehri, S., Badie Bostan, H. & Hosseinzadeh, H. Protective effect of crocin against d-galactose-induced aging in mice. *Avicenna J Phytomed* **8**, 14-23 (2018).
27. Lu, H.J. et al. Ruscogenin ameliorates diabetic nephropathy by its anti-inflammatory and anti-fibrotic effects in streptozotocin-induced diabetic rat. *BMC Complement Altern Med* **14**, 110 (2014).
28. Sova, M. & Saso, L. Natural Sources, Pharmacokinetics, Biological Activities and Health Benefits of Hydroxycinnamic Acids and Their Metabolites. *Nutrients* **12** (2020).
29. Heo, H.J. et al. Effects of oleamide on choline acetyltransferase and cognitive activities. *Biosci Biotechnol Biochem* **67**, 1284-1291 (2003).
30. Ano, Y. et al. Preventive effects of a fermented dairy product against Alzheimer's disease and identification of a novel oleamide with enhanced microglial phagocytosis and anti-inflammatory activity. *PLoS One* **10**, e0118512 (2015).
31. Wang, C. et al. Hydroxyeicosapentaenoic acids and epoxyeicosatetraenoic acids attenuate early occurrence of nonalcoholic fatty liver disease. *Br J Pharmacol* **174**, 2358-2372 (2017).
32. Nagatake, T. et al. 12-Hydroxyeicosapentaenoic acid inhibits foam cell formation and ameliorates high-fat diet-induced pathology of atherosclerosis in mice. *Sci Rep* **11**, 10426 (2021).
33. Rokicki, J. et al. Daily Carnosine and Anserine Supplementation Alters Verbal Episodic Memory and Resting State Network Connectivity in Healthy Elderly Adults. *Front Aging Neurosci* **7**, 219 (2015).
34. Cai, H., Wen, Z., Meng, K. & Yang, P. Metabolomic signatures for liver tissue and cecum contents in high-fat diet-induced obese mice based on UHPLC-Q-TOF/MS. *Nutr Metab (Lond)* **18**, 69 (2021).
35. Anderson, A. et al. 7-Ketocholesterol in disease and aging. *Redox Biol* **29**, 101380 (2020).
36. Kanter, R. & Caballero, B. Global gender disparities in obesity: a review. *Advances in nutrition* **3**, 491-498 (2012).
37. Bilstein, A., Heinrich, A., Rybachuk, A. & Mösges, R. Ectoine in the Treatment of Irritations and Inflammations of the Eye Surface. *Biomed Res Int* **2021**, 8885032 (2021).
38. Zhao, M. et al. Resolvin D2 and its receptor GPR18 in cardiovascular and

746 metabolic diseases: A promising biomarker and therapeutic target. *Pharmacol*
747 *Res* **195**, 106832 (2023).
748 39. Singh, P. et al. Taurine deficiency as a driver of aging. *Science* **380**, eabn9257
749 (2023).
750 40. Warden, C., Barnett, J.M. & Brantley, M.A., Jr. Taurocholic acid inhibits
751 features of age-related macular degeneration in vitro. *Exp Eye Res* **193**, 107974
752 (2020).
753 41. Wolf, P.G. et al. Effects of taurocholic acid metabolism by gut bacteria: A
754 controlled feeding trial in adult African American subjects at elevated risk for
755 colorectal cancer. *Contemp Clin Trials Commun* **19**, 100611 (2020).
756 42. Ur Rahman, S., Qadeer, A. & Wu, Z. Role and Potential Mechanisms of
757 Nicotinamide Mononucleotide in Aging. *Aging Dis* (2023).
758 43. Harrison, F.E. A critical review of vitamin C for the prevention of age-related
759 cognitive decline and Alzheimer's disease. *J Alzheimers Dis* **29**, 711-726 (2012).
760 44. Pelton, R.B. & Williams, R.J. Effect of pantothenic acid on the longevity of
761 mice. *Proc Soc Exp Biol Med* **99**, 632-633 (1958).
762 45. Ishiguro, K. Aging effect of blood pantothenic acid content in female. *Tohoku J*
763 *Exp Med* **107**, 367-372 (1972).
764 46. Dave, N. et al. Dietary choline intake is necessary to prevent systems-wide
765 organ pathology and reduce Alzheimer's disease hallmarks. *Aging Cell* **22**,
766 e13775 (2023).
767 47. Wang, J., Cao, B., Zhao, H. & Feng, J. Emerging Roles of Ganoderma Lucidum
768 in Anti-Aging. *Aging Dis* **8**, 691-707 (2017).
769 48. Kim, Y.J. et al. Oleanolic Acid Protects the Skin from Particulate Matter-
770 Induced Aging. *Biomol Ther (Seoul)* **29**, 220-226 (2021).
771 49. Ványolós, A. et al. Extracts and Steroids from the Edible Mushroom
772 Hypholoma lateritium Exhibit Anti-Inflammatory Properties by Inhibition of
773 COX-2 and Activation of Nrf2. *Chem Biodivers* **17**, e2000391 (2020).
774 50. Li, Z., Mu, C., Wang, B. & Jin, J. Graveoline Analogs Exhibiting Selective
775 Acetylcholinesterase Inhibitory Activity as Potential Lead Compounds for the
776 Treatment of Alzheimer's Disease. *Molecules* **21**, 132 (2016).
777 51. Murakami, S. et al. Taurine ameliorates cholesterol metabolism by stimulating
778 bile acid production in high-cholesterol-fed rats. *Clin Exp Pharmacol Physiol*
779 **43**, 372-378 (2016).
780 52. Jakaria, M. et al. Taurine and its analogs in neurological disorders: Focus on
781 therapeutic potential and molecular mechanisms. *Redox Biol* **24**, 101223 (2019).
782 53. Guy, J. & Peters, M.G. Liver disease in women: the influence of gender on
783 epidemiology, natural history, and patient outcomes. *Gastroenterol Hepatol (N*
784 *Y)* **9**, 633-639 (2013).
785 54. Guo, Q. et al. Taurine Attenuates Oxidized Fish Oil-Induced Oxidative Stress
786 and Lipid Metabolism Disorder in Mice. *Antioxidants (Basel)* **11** (2022).
787 55. Qi, W. et al. The ω-3 fatty acid α-linolenic acid extends Caenorhabditis elegans
788 lifespan via NHR-49/PPARα and oxidation to oxylipins. *Aging Cell* **16**, 1125-
789 1135 (2017).
790 56. Hajri, T., Pronczuk, A. & Hayes, K. Linoleic acid-rich diet increases hepatic
791 taurine and cholesterol 7α-hydroxylase activity in conjunction with altered bile
792 acid composition and conjugation in gerbils. *The Journal of nutritional*
793 *biochemistry* **9**, 249-257 (1998).
794 57. Wang, H. et al. Mutations in SREBF1, Encoding Sterol Regulatory Element
795 Binding Transcription Factor 1, Cause Autosomal-Dominant IFAP Syndrome.

Am J Hum Genet **107**, 34-45 (2020).
58. Birder, L.A. & Jackson, E.K. Dysregulated Purine Metabolism Contributes to Age-Associated Lower Urinary Tract Dysfunctions. *Adv Geriatr Med Res* **3** (2021).
59. Sekiya, M. et al. SREBP-1-independent regulation of lipogenic gene expression in adipocytes. *J Lipid Res* **48**, 1581-1591 (2007).
60. Liu, Y. et al. The Role of PPAR-δ in Metabolism, Inflammation, and Cancer: Many Characters of a Critical Transcription Factor. *Int J Mol Sci* **19** (2018).
61. Chatterjee, I. et al. Vitamin D receptor promotes healthy microbial metabolites and microbiome. *Sci Rep* **10**, 7340 (2020).
62. Penn, D.J., Zala, S.M. & Luzynski, K.C. Regulation of Sexually Dimorphic Expression of Major Urinary Proteins. *Front Physiol* **13**, 822073 (2022).
63. Lu, Y., Pang, Z. & Xia, J. Comprehensive investigation of pathway enrichment methods for functional interpretation of LC-MS global metabolomics data. *Brief Bioinform* **24** (2023).
64. Johnstone, T.C., Park, G.Y. & Lippard, S.J. Understanding and improving platinum anticancer drugs--phenanthriplatin. *Anticancer Res* **34**, 471-476 (2014).
65. Marcu, L.G. Gender and Sex-Related Differences in Normal Tissue Effects Induced by Platinum Compounds. *Pharmaceuticals (Basel)* **15** (2022).
66. Chen, W.Y. et al. Cisplatin Nephrotoxicity Might Have a Sex Difference. An analysis Based on Women's Sex Hormone Changes. *J Cancer* **8**, 3939-3944 (2017).
67. Nematbakhsh, M. et al. Gender difference in Cisplatin-induced nephrotoxicity in a rat model: greater intensity of damage in male than female. *Nephrourol Mon* **5**, 818-821 (2013).
68. Jiang, J. et al. Decoding the role of long noncoding RNAs in the healthy aging of centenarians. *Brief Bioinform* **22** (2021).
69. Kent, M.S. et al. Longevity and mortality in cats: A single institution necropsy study of 3108 cases (1989-2019). *PLoS One* **17**, e0278199 (2022).
70. Svedlund Eriksson, E. et al. Castration of Male Mice Induces Metabolic Remodeling of the Heart. *J Endocr Soc* **6**, bvac132 (2022).
71. Zhang, X., Thatcher, S., Wu, C., Daugherty, A. & Cassis, L.A. Castration of male mice prevents the progression of established angiotensin II-induced abdominal aortic aneurysms. *J Vasc Surg* **61**, 767-776 (2015).
72. Simopoulos, A.P. & Van Itallie, T.B. Body weight, health, and longevity. *Ann Intern Med* **100**, 285-295 (1984).
73. van de Wouw, M., Schellekens, H., Dinan, T.G. & Cryan, J.F. Microbiota-Gut-Brain Axis: Modulator of Host Metabolism and Appetite. *J Nutr* **147**, 727-745 (2017).
74. Ghosh, T.S., Shanahan, F. & O'Toole, P.W. The gut microbiome as a modulator of healthy ageing. *Nat Rev Gastroenterol Hepatol* **19**, 565-584 (2022).
75. McGee, J.S. & Huttenhower, C. Of mice and men and women: Sexual dimorphism of the gut microbiome. *Int J Womens Dermatol* **7**, 533-538 (2021).
76. Shin, M.S. et al. Long-term Surgical and Chemical Castration Deteriorates Memory Function Through Downregulation of PKA/CREB/BDNF and c-Raf/MEK/ERK Pathways in Hippocampus. *Int Neurourol J* **23**, 116-124 (2019).
77. Kim, J.Y., Yang, S.H., Kwon, J., Lee, H.W. & Kim, H. Mice subjected to uncontrollable electric shocks show depression-like behaviors irrespective of their state of helplessness. *Behav Brain Res* **322**, 138-144 (2017).

78. Kutlikova, H.H. et al. The effects of testosterone on the physiological response to social and somatic stressors. *Psychoneuroendocrinology* **117**, 104693 (2020).
79. Eshraghi-Jazi, F. & Nematbakhsh, M. Sex Difference in Cisplatin-Induced Nephrotoxicity: Laboratory and Clinical Findings. *J Toxicol* **2022**, 3507721 (2022).
80. Rostami, B. et al. Effect of testosterone on Cisplatin-induced nephrotoxicity in surgically castrated rats. *Nephrourol Mon* **6**, e21546 (2014).
81. Leifke, E. et al. Age-related changes of serum sex hormones, insulin-like growth factor-1 and sex-hormone binding globulin levels in men: cross-sectional data from a healthy male cohort. *Clin Endocrinol (Oxf)* **53**, 689-695 (2000).
82. Ederer, M.L. et al. Voluntary Wheel Running in Old C57BL/6 Mice Reduces Age-Related Inflammation in the Colon but Not in the Brain. *Cells* **11** (2022).
83. Lueptow, L.M. Novel Object Recognition Test for the Investigation of Learning and Memory in Mice. *J Vis Exp* (2017).
84. Xia, J. & Wishart, D.S. MSEA: a web-based tool to identify biologically meaningful patterns in quantitative metabolomic data. *Nucleic Acids Res* **38**, W71-77 (2010).
85. Alseekh, S. et al. Mass spectrometry-based metabolomics: a guide for annotation, quantification and best reporting practices. *Nat Methods* **18**, 747-756 (2021).
86. Luo, Y.M. et al. Insights into the mechanisms of triptolide nephrotoxicity through network pharmacology-based analysis and RNA-seq. *Front Plant Sci* **14**, 1144583 (2023).
87. Rong, S. et al. The TIM-1:TIM-4 pathway enhances renal ischemia-reperfusion injury. *J Am Soc Nephrol* **22**, 484-495 (2011).
88. Cox, M.P., Peterson, D.A. & Biggs, P.J. SolexaQA: At-a-glance quality assessment of Illumina second-generation sequencing data. *BMC Bioinformatics* **11**, 485 (2010).
89. Kim, D., Langmead, B. & Salzberg, S.L. HISAT: a fast spliced aligner with low memory requirements. *Nat Methods* **12**, 357-360 (2015).
90. Trapnell, C. et al. Differential gene and transcript expression analysis of RNA-seq experiments with TopHat and Cufflinks. *Nat Protoc* **7**, 562-578 (2012).
91. Kumar, L. & M, E.F. Mfuzz: a software package for soft clustering of microarray data. *Bioinformation* **2**, 5-7 (2007).
92. Lu, Y., Pang, Z. & Xia, J. Comprehensive investigation of pathway enrichment methods for functional interpretation of LC–MS global metabolomics data. *Briefings in Bioinformatics* **24** (2022).
93. Su, G.-H. et al. Radiogenomic-based multiomic analysis reveals imaging intratumor heterogeneity phenotypes and therapeutic targets. *Science Advances* **9**, eadf0837 (2023).

Author Contributions

J.J. conceived and designed this study; J.J. and W.W. wrote and revised this manuscript; S.Y. and F.L. provided necessary resources to this study; J.J. performed the metabolomics, RNA-seq analysis, and the western blot assay; N.G. and X.G performed the metabolomics analysis; Y.W. and G.W. performed the animal behavior tests; J. Q., and K. G. performed the sham/castration procedure; J.J., Y.W., G.W., J. Q., K. G., X.G and Y.L. did the mouse colony and tissue samples collection.

Acknowledgement

We acknowledge Ms. Jiahui Liu for her generous help for sample collection and Dr. Xinhui Liu for his kind help for assessing renal injury scores. This work was supported by Shenzhen Science and Technology Program (Grant No.RCBS20210706092341003) to J.J.

Declaration of interests

The authors declare that none of them have competing interests.

904 **FIGURES**

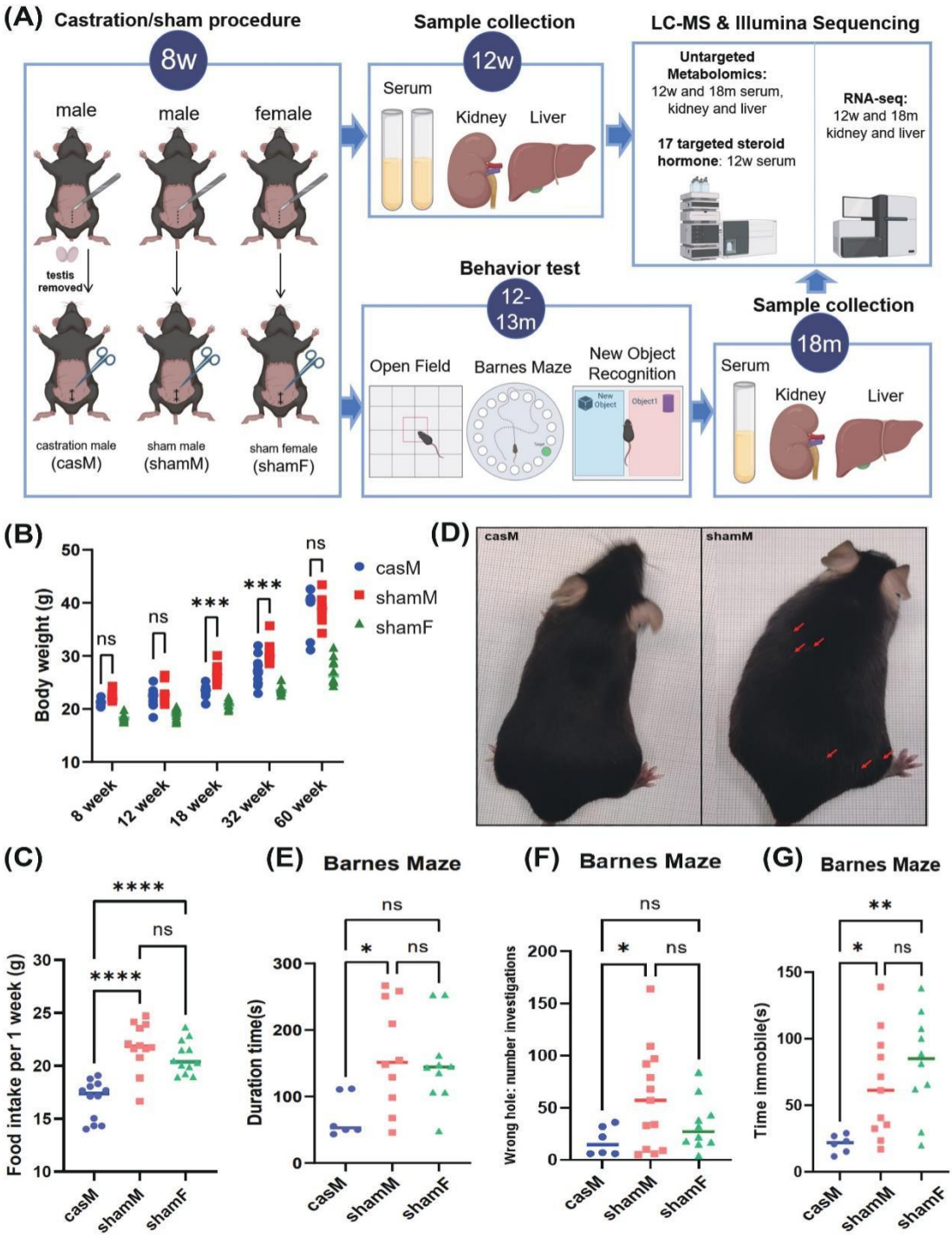

905

906 **Figure 1. Overall study design as well as phenotypic and behavior tests of**
907 **castration-mediated longevity.** (**A**) Graphic illustration of the overall experimental
908 design. (**B**) Body weight of casM, shamM and shamF mice from 8 to 60 weeks (n = 13,
909 12, 13 for casM, shamM, and shamF, respectively; unpaired students' t-test,***p <
910 0.001, ns: not significant) (**C**) Significant less food intake was observed in casM group
911 by One-Way ANOVA, ****p < 0.0001 (**D**) More gray hairs (see red arrows) were
912 observed in shamM than casM at 12-13 months old; (**D-F**) Analysis of BM tests results:

duration time that mice have spent to find the correct target escape hole (**D**), exploration of wrong holes numbers (**E**), and immobile time during the test (**F**) among casM (n=6), shamM (n= 13) and shamF (n = 10) by One-Way ANOVA, $*p < 0.05$, $**p < 0.01$, ns: not significant. For Figure 1C & E-G, Tukey correction was used for correction of multiple comparisons and median lines were shown.

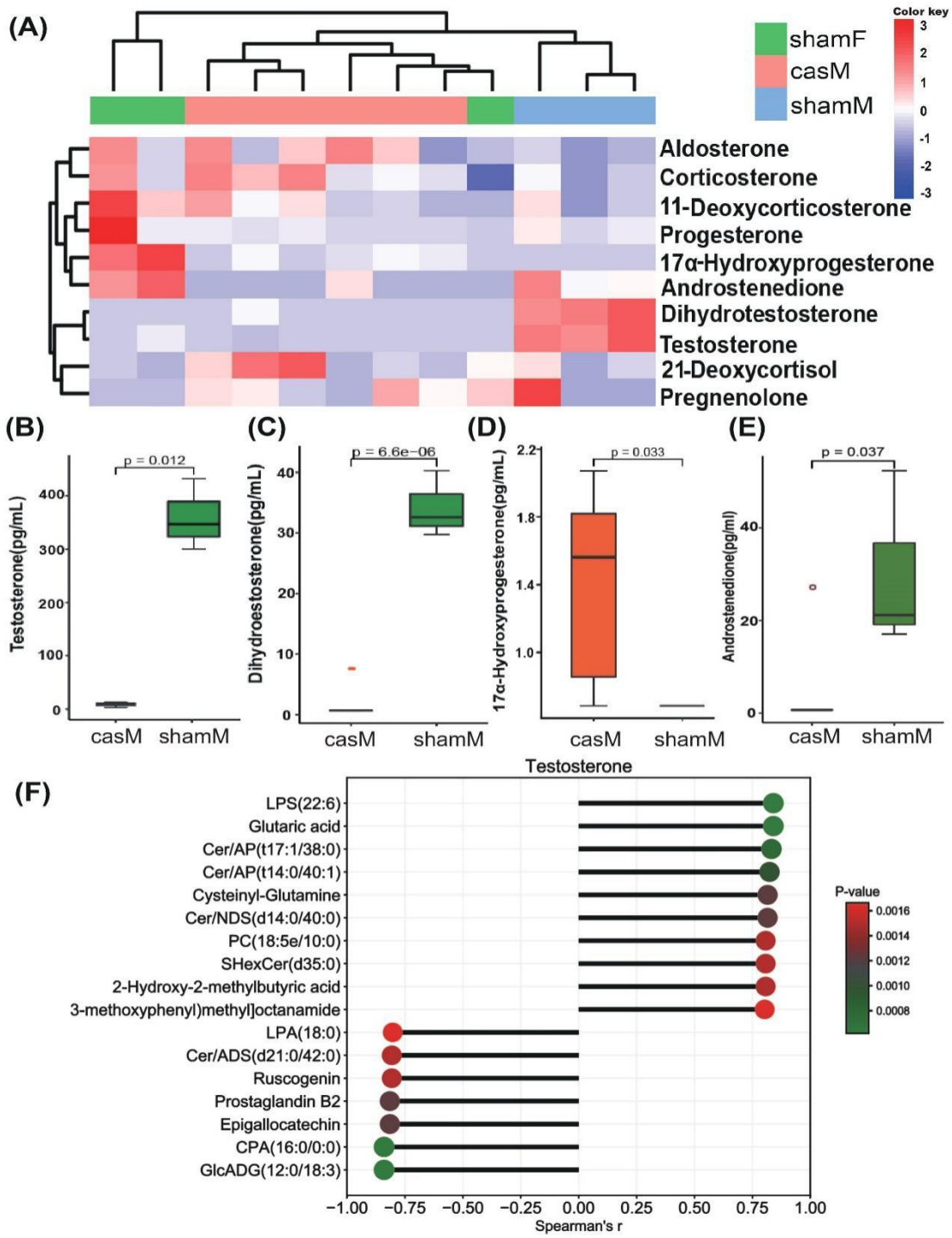

Figure 2. Alterations of the steroid hormones secretion induced by castration. (**A**) Hierarchical cluster heatmap of z-score standardized expression levels of 10 detectable steroid hormones among shamM, casM and shamF; (**B-E**) Comparisons of the quantitative levels of testosterone (**B**), dihydroestosterone (**C**), 17-hydroxyprogesterone (**D**) and androstenedione (**E**) between shamM and casM (unpaired students' t-test, *p*-values were shown on top); (**F**) List of compounds highly correlated with TS (Spearman's $|r| \geq 0.8$, $p \leq 0.001$). Median line was shown for B-E.

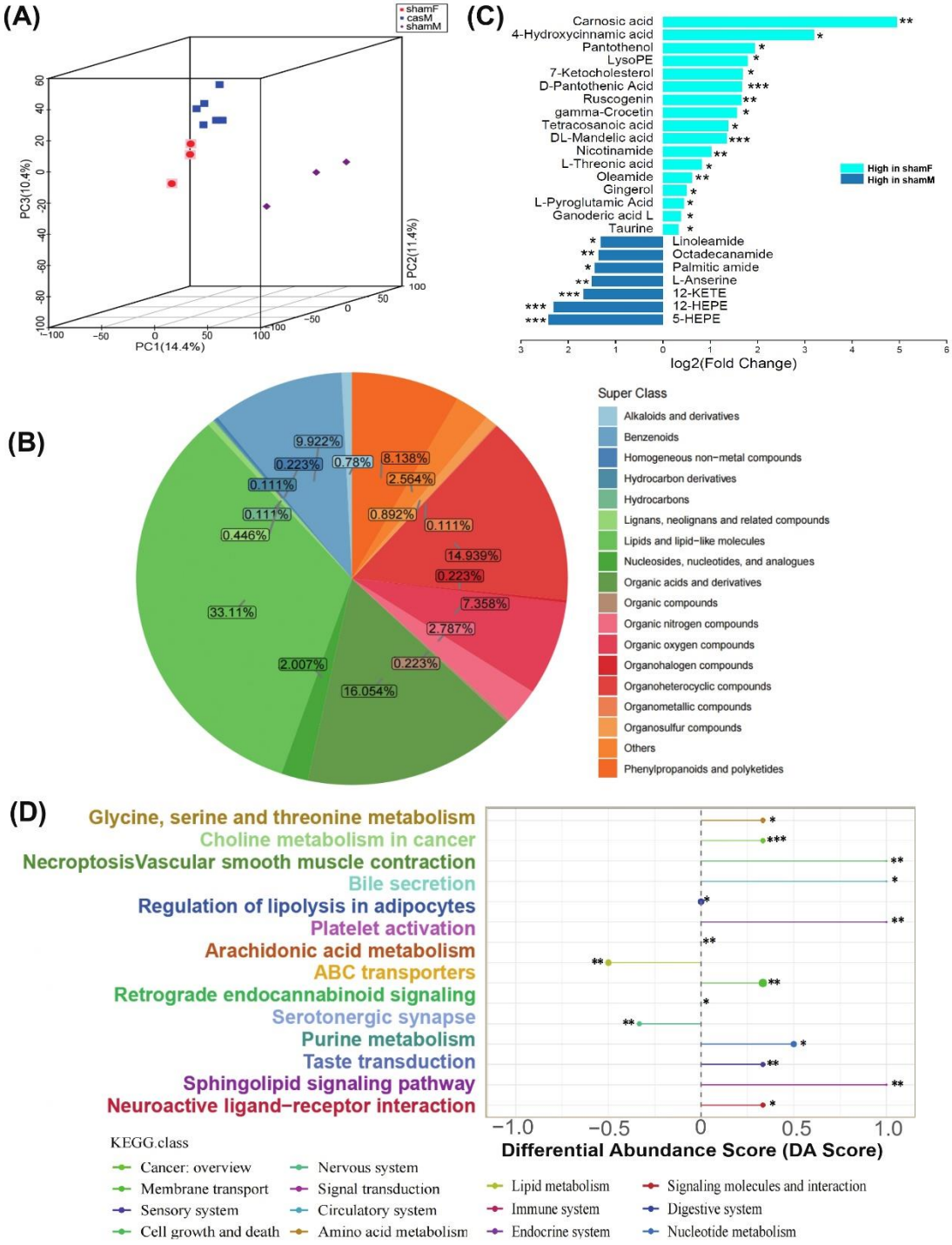

Figure 3. Characterizations of the 12w serum metabolomics. (**A**) PCA clustering of the serum untargeted metabolomics among casM, shamM and shamF; (**B**) Categories of the 1495 12w serum metabolites with high quality MS^2 annotations; (**C**) Representative SAMs between shamM and shamF that related with aging and healthy aging (unpaired students' t-test, $*p < 0.05$, $**p < 0.01$, $***p < 0.001$); (**D**) Differential abundance (DA) scores were calculated for the significant enrichment terms between shamM and shamF ($*p < 0.05$, $**p < 0.01$, $***p < 0.001$).

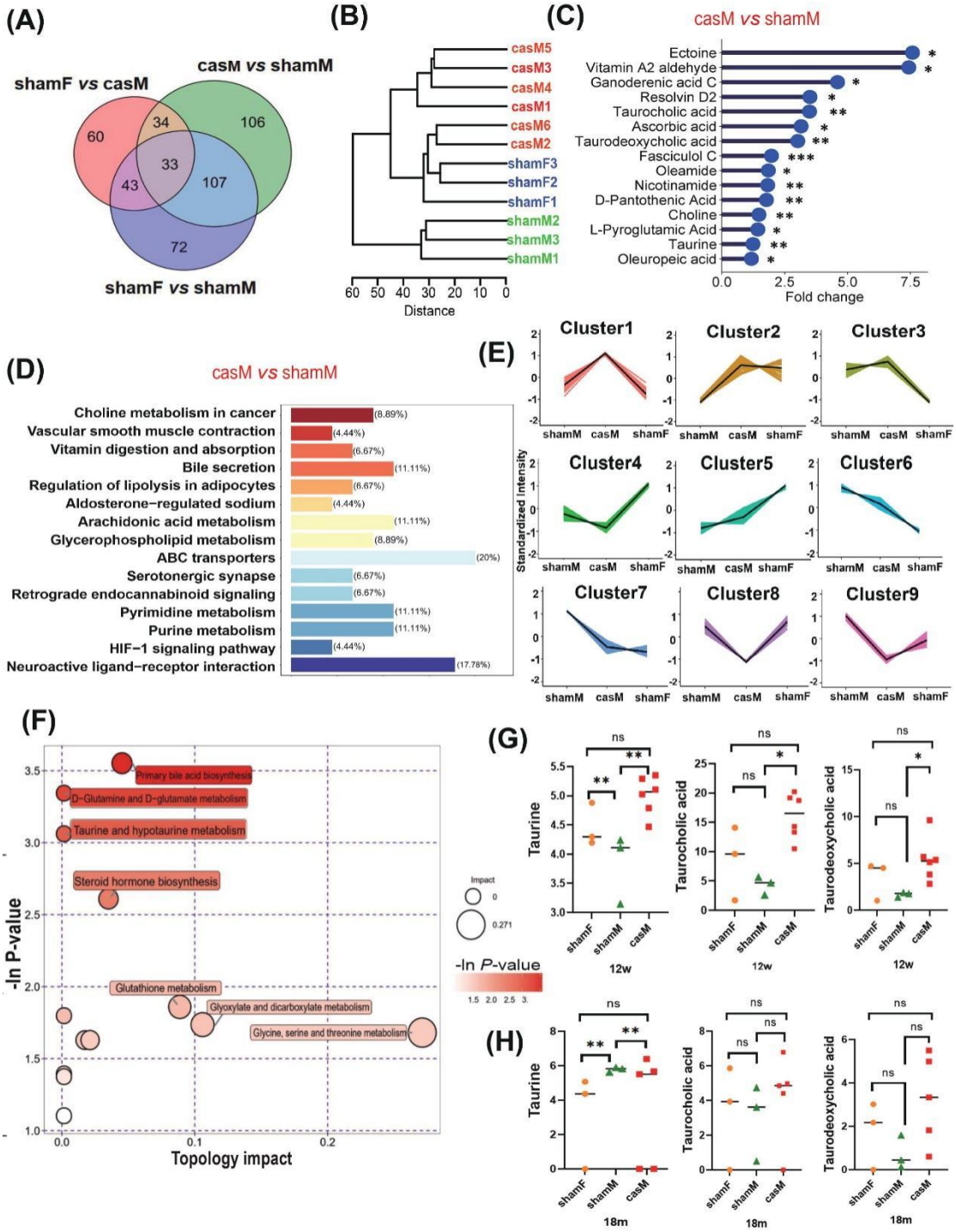

Figure 4. Identification of castration-specific metabolomic features in 12w mice. (**A**) Venny diagram of the serum SAMs identified from "shamF *vs* ShamM", "shamF *vs* casM" and "casM *vs* ShamM"; (**B**) Hierarchical clustering tree of different mouse groups using levels of compounds as input; (**C**) Representative food derived SAMs between casM and shamM (unpaired students' t-test, $*p < 0.05$, $**p < 0.01$, $***p < 0.001$); (D) Barplot of the KEGG enrichment terms using SAMs of "casM *vs* ShamM", percentage of hit compounds to total SAMs was calculated for each term; (**E**)

Expression patterns of merged SAMs among casM, shamM and shamF analyzed using mfuzzing clustering. Clusters 1 and 8 distinctively represent metabolites that are, respectively, highly and lowly detected specifically in casM. (**F**) Significantly enriched KEGG terms of metabolites highly expressed metabolites in casM (cluster 1 in **E**) calculated by topology-based pathway enrichment with topology impact shown in x-axis; (**G-H**) Comparisons of taurine, taurocholic acid and taurodeoxycholic acid among 12w (**G**) and 18m (**H**) shamF, shamM and casM (One-Way ANOVA, $*p < 0.05$, $**p < 0.01$, ns: not significant). For G and H, Tukey correction was used for correction of multiple comparisons and median lines were shown.

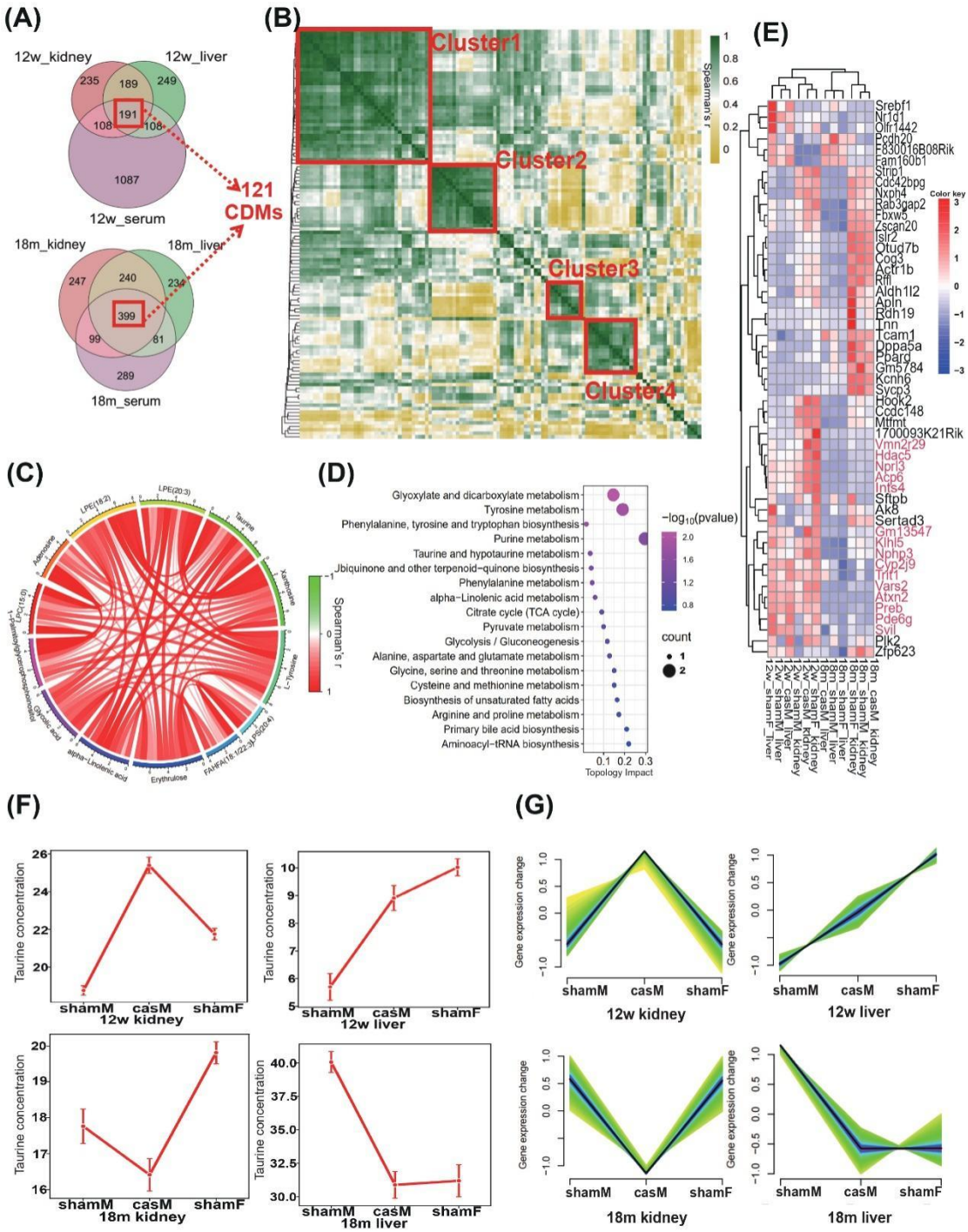

Figure 5. Co-expression analysis across serum, livers and kidneys identifies potential taurine-related regulators. (**A**) Venn diagram of detected compounds among serum, livers and kidneys across all the mouse groups at 12w and 18m, 121 commonly detected compounds (CDBs) were identified; (**B**) Co-expression analysis of the 121 CDBs revealed four major consensus clusters; (**C**) Correlation circos plot of the cluster 4 compounds in **B**; (**D**) Topology-based pathway enrichment analysis of the cluster 4 compounds in **B**, x-axis is the topology enrichment impact of hinted

compounds; (**E**) Hierarchical cluster heatmap of z-score standardized expression levels of 51 taurine related genes in 12w and 18m kidneys and livers among shamM, shamF and casM mice. Genes selectively reduced in 18m tissues are highlighted in red; (**F**) Trends of taurine levels with standard deviation (SD) among shamM, shamF and casM across liver and kidney tissues in 12w and 18m mice; (**G**) Mfuzzing clustering of the 51 taurine co-expressed genes across liver and kidney tissues in 12w and 18m mice.

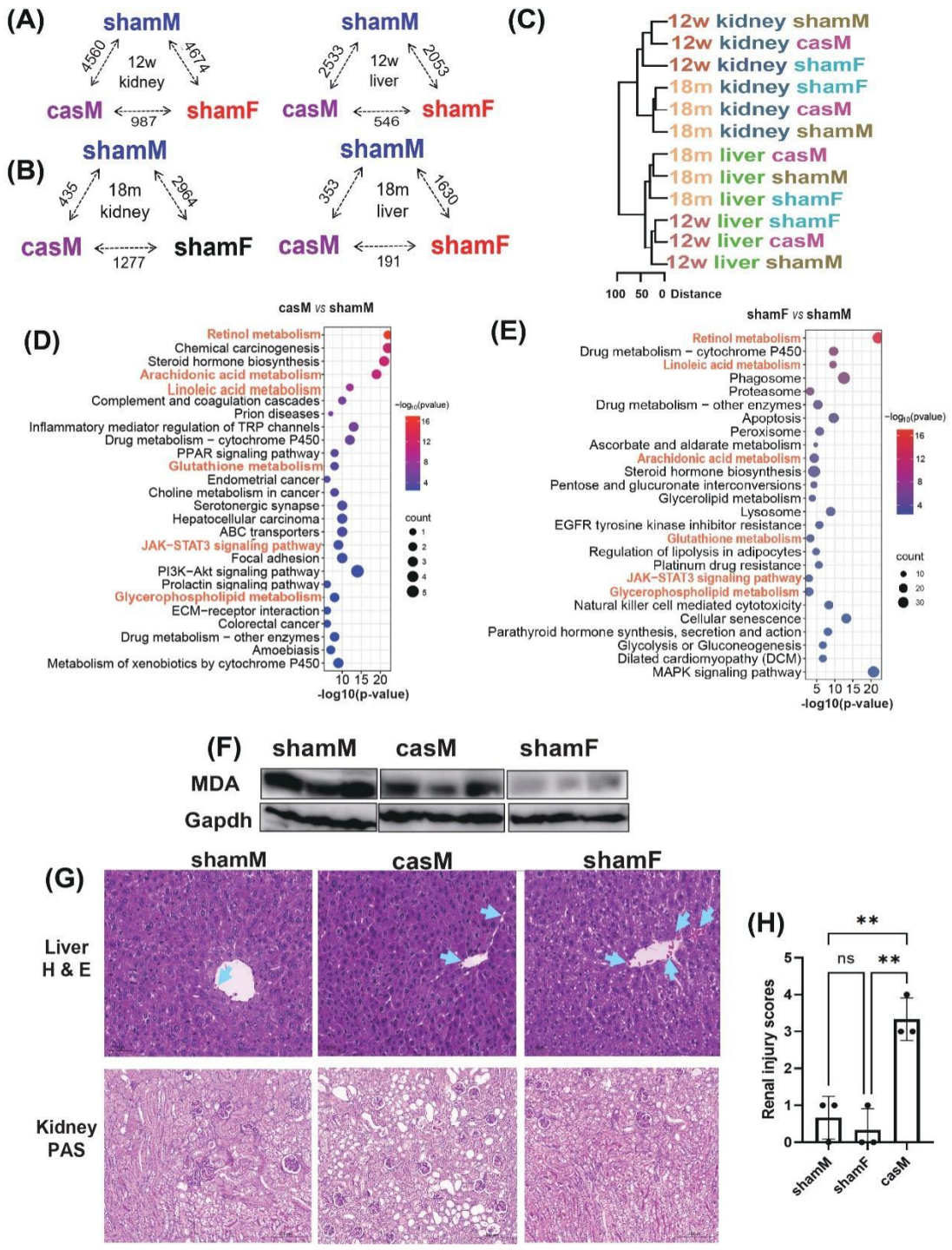

969

970 **Figure 6. Joint metabolomic-transcriptomic analysis reveals a stronger capacity of**
971 **defensing lipid peroxidation in female and castrated male.** (**A-B**) The numbers of
972 DEGs among livers and kidneys tissues of shamM, shamF and casM mice collected at
973 12w (**A**) and 18m (**B**); (**C**) Hierarchical clustering of 12w and 18m liver and kidney
974 samples demonstrating casM's closer alignment with shamF than sham; (**D, E**)
975 Representative significantly enriched KEGG pathways in 18m liver samples from
976 'casM *vs* ShamM,' (**D**) and 'shamF *vs* ShamM' (**E**), identified by joint transcriptomic-

977 metabolomic analysis using DEGs and SAMs. Pathways marked in orange indicate
978 common terms between these two comparisons. (**F**) Immunoblotting of MDA in 18m
979 livers; (**G**) H & E staining of livers (upper panel) and PAS staining of kidneys (lower
980 panel) in 12w mice (4 week post castration/sham procedure) with cisplatin treatment,
981 blue arrows indicate representative injury spots in livers; (**H**) Bar plots of renal injury
982 scores in three groups of mice by One-Way ANOVA test (Tukey correction was used
983 for correction of multiple comparisons, $^{**}p < 0.01$, ns: not significant).